

## Application of self-healing technique to fibre reinforced polymer wind turbine blade

Omosola Fifo, Kevin Ryan and Biswajit Basu\*

*Department of Civil, Structural & Environmental Engineering, Trinity College Dublin, Ireland*

*(Received August 14, 2014, Revised January 22, 2015, Accepted January 24, 2015)*

**Abstract.** This paper presents a novel concept of healing some of the damages in wind turbine blades (WTBs) such as cracks and delamination. This is achieved through an inherent functioning autonomous repairing system. Such wind turbine blades have the benefit of reduced maintenance cost and increased operational period. Previous techniques of developing autonomous healing systems uses hollow glass fibres (HGFs) to deliver repairing fluids to damaged sites. HGFs have been reported with some limitations like, failure to fracture, which undermines their further usage. The self-healing technique described in this paper represents an advancement in the engineering of the delivery mechanism of a self-healing system. It is analogous to the HGF system but without the HGFs, which are replaced by multiple hollow channels created within the composite, inherently in the FRP matrix at fabrication. An in-house fabricated NACA 4412 WTB incorporating this array of network hollow channels was damaged in flexure and then autonomously repaired using the vascular channels. The blade was re-tested under flexure to ascertain the efficiency of the recovered mechanical properties.

**Keywords:** wind turbine blade; self-healing; flexural stiffness; vascular network; fibre reinforced polymer

### 1. Introduction

Wind turbines have become a prominent clean energy source progressing more rapidly than other renewable energy technologies. An important component of these energy extracting devices are the rotor blades. The latest generation of the wind turbine blades (WTB) are designed to be robust, to withstand environmental challenges and operate at the optimum efficiency at their residing locations. The majority of these blades are built with either glass or carbon fibre reinforced polymer (FRP). These materials of light weight and high stiffness enable the turbines to operate at higher altitude, utilising the higher wind speed available at such heights.

In spite of having certain advantages in using FRP materials, there are associated difficulties, such as rapid structural and material disintegration. Structural dilapidation of WTBs is often a direct response to interior damages to critical layers or fibres within the blades' architecture. Over the past decade, blade failure has been a factor in many wind turbine failures around the globe (Young 2010). WTBs are complex and meticulously crafted structures required to be strong and light but can be highly susceptible to local stress concentration. To determine the extensive

---

\*Corresponding author, Professor, E-mail: [basub@tcd.ie](mailto:basub@tcd.ie)

influence of this phenomenon, full scale destructive tests are usually carried out. However, such comprehensive tests are often privately conducted, regarded as developmental research on wind energy and as a result, few studies have been published on the testing of WTBs to failure. Marín *et al.* (2009) examined a damaged 300 kW wind turbine blade. It was found that deep seated flaws and damages like inter-laminar separations-delamination, cracks and defects from the fabrication process played a prominent role in the damage event. The problems arising from inconsistencies in the manufacturing process often include resin deficiency areas, abrupt change in laminate thickness, misalignment and fibre disorientations. WTBs are structurally analysed as a cantilever beam, subjected to a varying load (wind), load reversal and non-uniform loading (self weight). Due to these uncertainties and the complex loading conditions, WTBs have high tendency of developing stress concentration at the root section, where the bending moment is maximum. At the start of this section is the maximum chord length where the blade is connected to the steel hub and the smallest angle on the blade profile. A design flaw in this region creates a local stress concentration that grows over time while fatigue sets in. A sharp change of angle around the maximum chord length causes re-entrant corner effects and gives rise to irregularities in "stress distribution" (Timoshenko 1941). Also, change in laminate thickness causes load transmission eccentricity. This induces bending moments thereby adversely affecting the effectiveness and stability of the laminate operations (Marín *et al.* 2009).

Research carried out on blades (Overgaard *et al.* 2010, Shokrieh and Rafiee 2006, Sundaresan *et al.* 1999) showed that a critical zone exists on WTBs often accompanied with high probability of failure. As a result, a WTB is more likely to suffer damage in between the root section and the quarter to third length of the blade's span. Around this region, WTBs undergo a rapid change in their cross-sectional area. This section contains a huge portion of the spar, which controls the structure's ultimate strength. Sundaresan *et al.* (1999) recorded buckling failure of the spar web preceded by delamination at a location of 37.5% along the blade from the root. Shokrieh and Rafiee (2006) also found that a critical zone lies in compression flange on the spar. Cracks and delamination irrespective of their size or type in this region make a vulnerable structure, highly prone to sudden failure under operation.

The use of the latest structural health monitoring (SHM) devices, appended to the critical region on the blade could be essential in averting catastrophic failure. Currently, in the event of detecting a potential damage site such as delamination, the blades are often repaired through scarf repair and plug/patch methods (Found and Friend 1995, Lekou and van Wingerde 2006). Likewise, the use of bonding pins perpendicularly driven through the delaminated area have been reported (Li *et al.* 2006). Given the uncertainty of the damage detection, these repair techniques will be costly for components of large scale structures such as WTBs, which have accessibility issues associated with nacelle height. In particular for the case of off-shore WTBs, installation in remote locations adds significantly to the maintenance costs (Larsen 2009). Therefore, timely maintenance of WTBs leads to cost reduction and ensures further sustainability. In order to have a swift response to damage and internal micro failure, this paper proposes the integration and the incorporation of a self-healing system into FRP WTBs.

Autonomous self repair of FRP structures has been an actively researched topic over the last decade, (Caruso *et al.* 2008, Kessler and White 2001, Motuku *et al.* 1999; Norris *et al.* 2011, Trask and Bond 2006). This system, however, has not been applied to repair damages within areas of stress concentration on a WTB. Self-healing or repair gives a dual or multifunctional ability to the host structure. It enables the structure to carry out its primary function while simultaneously being at liberty to initiate a repairing procedure. The latest generation of self healing requires the use of

two or three dimensional vascular system for delivery mechanism (Blaiszik *et al.* 2010, Williams *et al.* 2008). The delivery structure, often made up of hollow glass fibre (HGF), provides an efficient method of transporting a repairing agent or the healing fluid within the incorporating structure. The system provides a global coverage and accessible paths for the repairing agent.

A report by Bleay *et al.* (2001) on HGFs was widely accepted and many had based their studies on the finding that HGFs are not mechanically detrimental to the functionality of their host. *Two-dimensional* or *three-dimensional* HGFs pose different challenges of their own. A particular threshold of energy is required to cause a penetrating crack through the hollow fibres before the healing can be activated. It has also been reported that due to impediments on the crack by HGFs debris, polymerisation of the repairing agent was activated inside the embedded fractured HGF container. Also, disparity in mixing with the hardener (for a two healing system), a prerequisite condition for self-healing has also been reported (Pang and Bond 2005; Williams *et al.* 2008).

The procedure proposed in this paper and reported in the subsequent sections describes an alternative technique to HGF vascular system incorporated in a WTB. It involves the creation of hollow network passages within the material architecture at the fabrication stage. The laminate constituting matrix forms the walls of a series of hollow sections similar to the walls formed using ink writing-scaffolding 3D network formation (Lewis 2006). This technique has been applied to small glass/polyester laminate coupons subjected to flexural loading (Fifo *et al.* 2014). The hollow networks are created using temporary insertions of removable material. The transient materials are removed from the finished product either through a chemical reaction process or by any available easy mechanical means, with minimum damage initiated in the material. The vacuum left behind by the insertions act as the delivery passages allowing the repairing agent to flow and penetrate damage sites within the material. This is similar to the use of HGF to store and deliver a repairing agent to the required location. The system described here does not require on-board storage of healing chemical, rather the repairing fluid is pressurised through the matrix walls from a supply reservoir. This creates a network of healing agent supply channels, eliminating undue obstruction of the adhesive from reaching the crack surfaces. Also, it creates more repairing avenues for cracks, which would otherwise have insufficient threshold energy to fracture a HGF, thereby increasing the recovered efficiency.

## 2. NACA 4412 WTB Features

Small sized wind turbines are often operated with blades of NACA 4412 aerofoil model. Some of these wind turbines have permanent magnetic generator (PMG) in place (Campos *et al.* 2001, Mishnaevsky Jr *et al.* 2011). At 5 m/s wind speed, such turbines are capable of generating up to 80 watts at 286 rpm. A typical blade is 700 mm in length with chord lengths of 168 mm and 68 mm at the root and at the tip respectively. These blade dimensions were chosen due to the suitability of short length for a Zwick Roell test rig, and for ease of fabrication—due to the linearity at both leading and trailing edges from the root to the tip. Also, it has less complex twist along the length of the aerodynamic shell. Aside from the physical characteristic, the NACA 4412 blade profile has been reported to have some aerodynamic advantages over other aerofoil types. The profile enables more efficient operation of the turbine in terms of higher power output, a result of coherent relation between the power coefficient,  $C_p$  to tip speed ratio (TSR) (Maalawi 2011). Also, Kurtulmus F. *et al.* (2007) reported the lift rate, at a set angle-of-attack of NACA 4412 blade to be much higher than those of NACA 0012 and NACA 23012.

### 2.1 Two-dimensional hollow network

Some studies (Kim *et al.* 1996, Tay *et al.* 2008) on the progressive failure analysis (PFA) of FRP composites have shown that under a specific loading condition, the most vulnerable layer(s)—the first ply failure (FPF)—within an FRP laminate can be identified. Similarly, results available from some of the few destructive testing on WTBs have been shown that the section, at a third of the blade's length from the root, is susceptible to failure (Shokrieh and Rafiee 2006, Sundaresan *et al.* 1999). Based on these findings, the 2D hollow networks in the GFRP NACA 4412 blade were strategically placed at the 2nd and the 6th layers from both top and bottom of the blade. The network was centred at 230 mm length of the blade from the root, covering an area of 0.025 m<sup>2</sup>. Each level of the multiple hollow networks was formed by connections between six evenly spaced longitudinal hollow spaces and five transverse hollow spaces, Fig. 1. A temporary formwork, in this case a 450 µm diameter nylon cable (fishing line) was used in creating the hollow space. The nylon cable was chosen due to its high loading capacity of 110 N. The cables were extracted after the laminate had cured. The network's coverage is the area enclosed by the intersections of the longitudinal and the transverse channels as shown in Fig. 1.

## 3. Fabrication of NACA 4412 WTB Aerofoil

A wooden blade was made from a piece of softwood, as shown in Fig. 2. A timber block was divided into 14 stations and each division was chiselled down to its appropriate aerofoil NACA 4412 profile. Thereafter, the prototype was placed in a silicon based moulding agent (Mold max-30) on which the top-half of the blade was imprinted. The mould mixture was allowed to cure for 24 hours before the wooden blade was taken out. The edges of the silicon mould were subsequently redressed to enhance workability.

The top half of the WTB was fabricated in a sequential fashion. Fifteen layers of E-class, woven roven, 200 g/m<sup>2</sup> of glass-fibre (Tissu 200 TB, Chromarat) were cut into a trapezoid like shape of the blade. In general, most small WTBs are isotropic in their mechanical properties and for this feature to be present; eight of the layers were cut in their primary orientation of [0°/90°]. The remaining seven were cut out such that they were at [±45°] to their primary orientation. The blade was fabricated with alternating layers of the stated orientations. A 630 g of Crystic 2446PALV orthophthalic polyester resin (Scott Bader) was apportioned in a 2.5:1 ratio by weight with the glass fibres according to the manufacturer's recommendation. Also, 12.6 g of organic peroxide methyl ethyl ketone peroxide (MEKP) was added to the polyester resin as the polymerising agent.

The silicon mould and the nylon cables were coated extensively with a de-moulding agent to facilitate post curing detachment of the blade from the mould and removal of the nylon wires from the FRP blade. Afterwards, a small volume of freshly prepared polyester matrix was spread evenly on the mould using a paint brush followed by a careful placement of the first layer [0°/90°]. This procedure was repeated for the second layer but with the layer oriented at [±45°]. At this point the nylon cables which had been attached to Balsa wood (at one end), at a specified distance from one another were placed on the matrix-soaked glass fibre clothing. The wires were held in position via slits cut into the mould at the appropriate positions as shown in Fig. 3 and Balsa wood pegs were used to apply and hold tension. The layering process was then resumed along with the appropriate fibre orientations. The process was only stopped briefly for the placement of the nylon cables on the 6th, 9th, and 13th layer. The blade was allowed to cure for 24 hours in the mould at room

temperature after which it was removed.

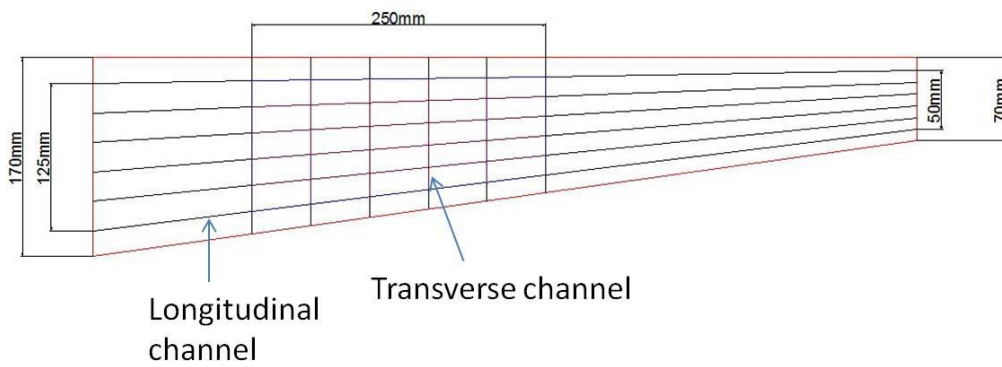


Fig. 1 NACA 4412 WTB 450  $\mu$ m hollow network layout



Fig. 2 Wooden NACA 4412 WTB prototype



Fig. 3 Slits cut into the mould, holding the 2D network formwork - nylon cables

The FRP blade was further cured for the same period and under the same conditions. Afterwards, the transversely placed nylon wires were removed. Initial attempts at drawing-out the longitudinal wires failed due to mass contraction of the matrix on the cables. The blade was heated in a Memmert oven at 80°C for 45 minutes to reduce the contraction stress. This thermal treatment, which was below the degrading temperature (Avila *et al.* 2008), allowed the coated material around the cables to melt thereby reducing frictional effects between the matrix walls and the cable ensuring successful removals.

#### 4. Mechanical tests

The flexural bending test was carried out on the blade using a Zwick Roell 1474 test machine. The set-up is as shown in Fig. 4. The test was conducted in displacement control mode at a rate of 2 mm/min using a 10 kN load cell. The maximum load limit and extension were set to 2 kN and 30 mm respectively. The automatic shutdown threshold was adjusted to 50% drop in the peak load. The test was conducted such that the load was held on following the termination of the test. The blade was simply supported at the root and at 57% of its length by two timber frames with a 300 mm span. This arrangement allows the third-length of the blade from the root, which is covered by hollow network to be specifically tested. The wooden blocks were sculptured to fit the blade's cross-sectional profile at their respective positions. This arrangement enabled the loading head of the Zwick Roell to be placed directly above the centre of hollow network passages. The blade was loaded from the inside rather than from the outside (the suction side), Fig. 4. Also in a similar fashion to the supports, a small timber piece was placed at the loading point for load distribution across the blade's width. The blade was trimmed off by 5 mm at the root section to eliminate curvature, which had developed during fabrication to avoid hindering the adhesive passage during repair. The surface exposed following the cut was subsequently cleaned with acetone. All the transverse hollow outlets were not used as the repairing agent's inlet points and were subsequently blocked with a silicon gel.



Fig. 4 Set up: Flexural testing of NACA 4412 WT B

The silicon was allowed to set and cure for 2 hours before the flexural testing. After concluding the initial flexural test, the blade was immediately loaded again to confirm a reduction in flexural modulus due to induced damage. Thereafter, the blade was injected with a cyanoacrylate (CA) adhesive, using the topmost longitudinal hollow inlets at the root as the injection points. The CA healing agent is a single part colourless adhesive and it is of low viscosity, achieving high strength within a few hours. The polymerisation of this adhesive can be activated by the presence of atmospheric moisture or hydroxide ions (Petrie 2007) making it suitable for this experiment. After injecting the CA adhesive into the blade, it was allowed to cure for 24 hours at room temperature. Afterwards, the post-repair test was conducted. The equivalent flexural stiffness,  $EI$ , of the blade at every stage and the efficiency,  $\eta$ , of the repair procedure were computed according to the Eqs. (1) and (2) respectively.

$$EI = \left( \frac{\Delta P}{\Delta \delta} \right) \frac{L^3}{48} \quad (1)$$

$$\text{Efficiency, } \eta = \frac{EI_{\text{postrepair}}}{EI_{\text{original}}} \times 100\% \quad (2)$$

In Eqs. (1) and (2),  $P$  is the applied load,  $\delta$  is the deflection at the mid-span and  $L$  is the length of the support span. Due to the non-linear behaviour of polymer plastics, the slopes were obtained using the secant method. The notations  $\Delta P$  and  $\Delta \delta$  denote changes in the applied load and deflection respectively from which the slope is obtained.

The flexural stiffness in Eq. (1) is based on Euler-Bernoulli beam theory for long and slender beams. It is envisaged that the equation will overestimate the stiffness values given the span length is approximately twice the width of the blade. However, the influence of this on the overall result is negligible given the consistency at all stages namely, the original, damaged and post-repair. Also, the total cross-sectional area of the hollowness at the root of the blade makes approximately 0.3% of the blade's root. Furthermore, the entire volume of the hollow network represents approximately 0.5 % of half of the blade's volume. This volume was adjudged not to be structurally detrimental.

## 5. Results and discussion

### 5.1 Initial test and adhesive inflow

Before the main test, trial runs of the proposed test were conducted to ensure that the blade fits the experimental set-up and that there is no slack leading to force without deformation. The immediate post-test visual examination following the damaged confirmation test, revealed a delaminated area (Fig. 7), near the loading head of the testing apparatus. This damage is located between the second and third layer below the loading head. This is attributed to the presence of the hollow network not matching the curved profile of the layers. As a result, more resin was used in the fabrication process, which created a weakened section between the layers. The load-deflection plots for all the different cases are presented in Fig. 5. The 'original' plot shows the blade's behaviour from its elastic range to failure stage indicated by the apparent non-linear deformation in between 8 mm and 25 mm. The other plot, 'damaged', confirms that the blade has been damaged. The curve

('damaged') shows a complete deviation from the plot, 'original', right from the onset of loading. It appears that permanent non-linear deformation had been induced into the blade as shown by the distinctive behaviour of the blade for the 'original' and for the 'damaged' test cases. This is further reiterated by the elastic flexural stiffness values of approximately  $87 \text{ Nm}^2$  and  $55 \text{ Nm}^2$  calculated at a load of 1000 N for the 'original' and the 'damaged' curves respectively, using the secant modulus as shown in Fig. 6. The difference in the flexural stiffness values shows that the blade had lost approximately 35% of its flexural stiffness.

Furthermore, the deformation around the average peak load of 1800 N of the 'original' plot defines the damage state of the blade in Fig. 5. The change in the normally expected flexural failure mode from sudden load drop to less brittle non-linear deformation in the plot can be attributed to the manner in which the load was being distributed. There was no flexural failure observed which would lead to failure of the bottom layers first. The timber block employed allowed the load to be further spread around it. Consequently, this led to the delamination around the weaker region of the blade near the loading timber and the trailing edge (Fig. 7). The failure cause is not definitive but can be attributed to a wider spread of stress at the loading point and the presence of the hollow network. Also, the asymmetric geometry of the blade may have contributed to this damage due to the stiffness discontinuity.

A total volume of 5.5 ml of the cyanoacrylate adhesive was manually injected into the blade while the load was still held on it. The load was taken off after the adhesive injection had been completed. The influx of the adhesive was started from the first injection point, in the second column near the trailing edge. This was to enable the adhesive a short travel route to the delaminated site. Droplets of the adhesive were observed at the nearest previously sealed transverse hollow section in the adhesive's path. This confirms that both the transversely and longitudinally oriented hollow sections were well connected and that the transverse hollow passages were not sufficiently sealed by the silicone sealant. Also, outward seepage of the adhesive was observed at the neighbouring injection points. The adhesive quickly covered a large area of the injecting surface making it difficult to locate some of the inlet points. Due to this, the majority of the holes were not used. Also, while attempting to locate unblocked injection points, the adhesive was noticed to have cured inside some of the syringe needles and on the injecting surface. Fig. 8 shows a schematic representation of the inlets at the blade's root. Furthermore, outflow of the cyanoacrylate adhesive was noted at the blade's tip. Traces of the outflow path were observed on the blade from the tip to the mid section where the blade was being loaded, Fig. 9.

Close to concluding the 'damaged' test run, there was a sudden increase in load due to the maximum deflected part of the blade at the loading point making contact with the steel base on which the wooden side supports were placed. This led to a 15 mm cut on the underside of blade near the loading timber, Fig. 10a. The cut was at the leading edge and also led to a significant bending which tilted up the blade's tip. Outflow of the adhesive was also noted at this damaged site.

## 5.2 Post-repair

The post-repair mechanical test response of the NACA 4412 blade is shown in Fig. 5. This figure clearly demonstrates the influence of the CA adhesive in aiding considerable recovery of the blade's stiffness. The flexural stiffness of the repaired blade within the elastic region (between 100-700 N) revealed a stiffness recovery of approximately  $72 \text{ Nm}^2$ . This stands at approximately 84% of the initial flexural stiffness. The recovered efficiency and the comparison plots in Fig. 5

indicate that the adhesive was solely responsible for the linear portion of the 'post-repair' plot. Beyond the elastic region, the adhesive's bond strength dwindles as the blade gradually reverted to its normal non-linear damaged behaviour.

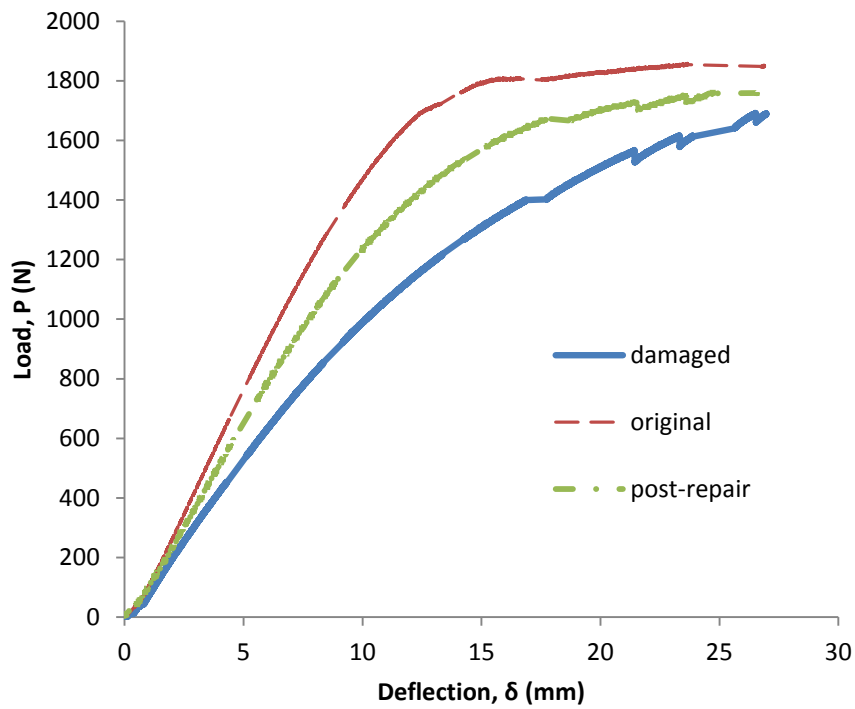


Fig. 5 Post-repair and Initial bending test results on NACA 4412

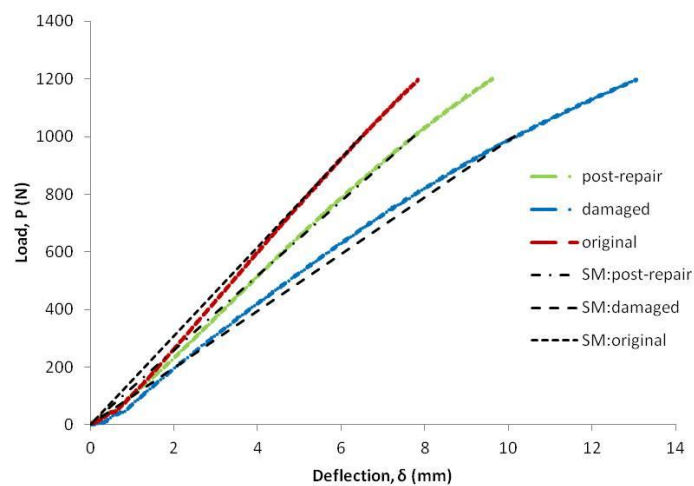


Fig. 6 Gradient determination using secant method



Fig. 7 Delaminatinon around the loading timber

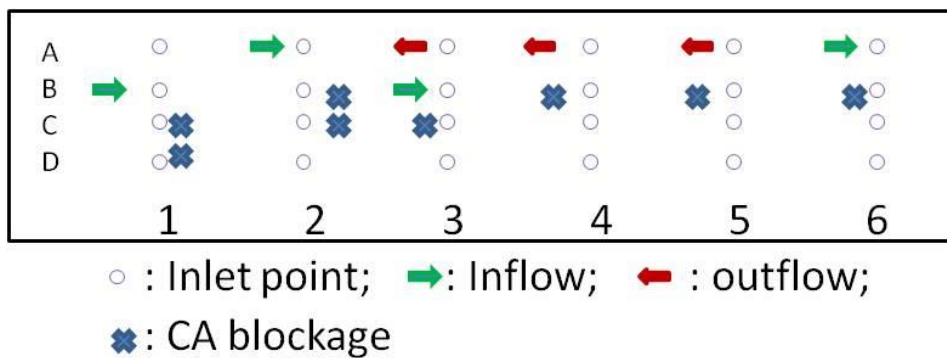


Fig. 8 Schematic illustration of the injecting point at the blade's root



Fig. 9 The cyanoacrylate adhesive's flow path from the blade's tip



(a) Damaged edge

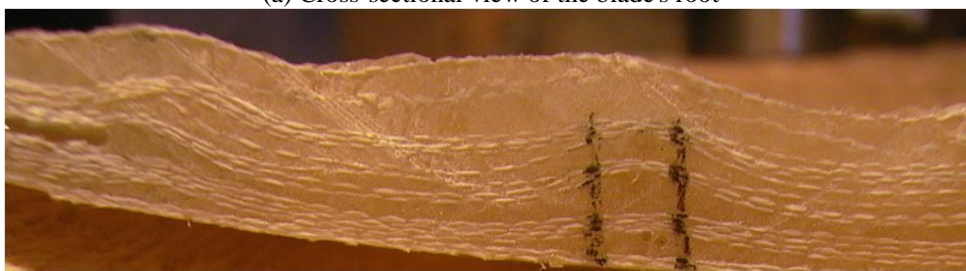


(b) Closer view of the damage with an outflow of the healing agent

Fig. 10 Underside cut on NACA 4412 and the tilting effect



(a) Cross-sectional view of the blade's root



(b) Enlarge view of the of the curvatures

Fig. 11 Curvature and imbalance resin volume across the width and depth

The post-repair failure was of similar nature to the pre-repair one but the underside cut experienced further damage. Therefore, it can be said that successful adhesive injection from the first row, closer to the loading plane, was instrumental in repairing some of the delamination. Though it was not quantified by the area it may have covered/healed, the adhesive was observed

flowing into the delaminated area. This in effect contributed to the overall recovery of the blade.

The results provide validation of the concept that a complex WTB structure can accommodate a self-healing system. The NACA 4412 WTB was the first of its kind to be fabricated with an embedded self-healing system and therefore it was expected to possess some flaws. A cross-section at the blade's root revealed an imbalanced resin concentration across the width and depth of the section, especially after each placement of the nylon cables (Fig. 11). Also, the figure shows curvatures around the nylon cables. These curvatures can be attributed as one of the factors that led to the delamination on the blade around the loading area. Under this current self-healing technique, curvature around the hollow sections will be inevitable but should be minimised. Generally, the fabrication process can be improved, using a prefabricated casing that allows the hollow-preforming materials in the transverse direction and those along the edges to be placed at appropriate angles.

## 6. Conclusions

The experiments in this paper were set out to examine a novel concept of introducing self-healing to a WTB. At this early stage of this type of repairing technique, the healing is a "one-shot" process. This makes it difficult to get a significant data set. The tested WTB was made in-house with 15 layers of glass/polyester and was laced with 450  $\mu\text{m}$  (diameter) 2D hollow networks at 2nd, 6th, 9th and 13th layer. The hollow network of vascular system, at each layer had a 0.025  $\text{m}^2$  coverage of the blade's surface area centred at a third of the blade's length from the root. Under flexural bending test, delamination was observed near the loading point. The cause was attributed to stress concentration. No flexural failure was observed. Rather the damaged blade was observed to have experienced some changes from linear to non-linear behaviour. This was confirmed upon reloading and it was evident as the flexural stiffness was reduced from 94  $\text{Nm}^2$  to 62  $\text{Nm}^2$ . This represents a 35% reduction in flexural stiffness. However, 84% of the initial stiffness was recovered in the post healing stage upon infusing some of the inlet channels of the network with a small volume of CA adhesive. The mechanical properties after the repair were largely similar to that of the initial state within the elastic limit. Beyond the elastic range, the blade simply reverted to its non-linear mode. This clearly shows that the mechanical behaviour of the blade in the post-repair stage will be comprehensively dependent on the repairing agent. The CA repairing fluid was observed flowing towards the delaminated area without significant hindrance, verifying that the hollow section was effective in delivering the adhesive to the delaminated site. Optimisation of the repair technique is possible by eliminating the curvature induced by the nylon formwork and investigating the adhesive viscosity.

## Acknowledgements

The authors would like to thank the Irish Research Council and Henkel Ireland R&D for funding this project. Also, special thanks to Mr Simon Murphy of Henkel Ireland R&D for his support and advice.

## References

- Avila, B.M., Dembsey, A.N., Kim, E.M., Lautenberger, C. and Dore, C. (2008), "Fire characteristics of polyester FRP composites with different glass contents", *Compos.Res. J.*, **2**(2).
- Blaiszik, B.J., Kramer, S.L.B., Olugebefola, S.C., Moore, J.S., Sottos, N.R. and White, S.R. (2010), "Self-healing polymers and composites", *Ann. Rev. Mater. Res.*, **40**(1), 179-211.
- Bleay, S.M., Loader, C.B., Hawyres, V.J., Humberstone, L. and Curtis, P.T. (2001), "A smart repair system for polymer matrix composites", *Compos. Part A: Appl. S.*, **32**(12), 1767-1776.
- Campos, T.S., Fernando, S. and Piggott, H. (2001), "Wind rotor blade construction", I. P. A. t. Poverty, (ed.). City.
- Caruso, M.M., Blaiszik, B.J., White, S.R., Sottos, N.R. and Moore, J.S. (2008), "Full recovery of fracture toughness using a nontoxic solvent-based self-healing system", *Adv. Funct. Mater.*, **18**(13), 1898-1904.
- Fifo, O., Ryan, K. and Basu, B. (2014), "Glass fibre polyester composite with in vivo vascular channel for use in self-healing", *Smart Mater. Struct.*, **23**(9), 095017.
- Found, M.S. and Friend, M.J. (1995), "Evaluation of CFRP panels with scarf repair patches", *Compos. Struct.*, **32**(1-4), 115-122.
- Kessler, M.R. and White, S.R. (2001), "Self-activated healing of delamination damage in woven composites", *Compos. Part A: Appl. S.*, **32**(5), 683-699.
- Kim, Y., Davalos, J.F. and Barbero, E.J. (1996), "Progressive failure analysis of laminated composite beams", *J. Compos. Mater.*, **30**(5), 536-560.
- Kurtulmus, F., Vardar, A. and Izli, N. (2007), "Aerodynamic analyses of different wind turbine blade profiles", *J. Appl. Sci.*, **7**(5), 663-670.
- Larsen, K. (2009), "Recycling wind turbine blades", *Renew. Energ. Focus*, **9**(7), 70-73.
- Lekou, D.J. and van Wingerde, A.M. (2006), "Repair techniques for composite materials applicable to wind turbine blades", *Proceedings of the 27th Riso International Symposium on Materials Science: Polymer composites materials for wind power turbines*. City: Riso National Laboratory, Roskilde, Denmark.
- Lewis, J.A. (2006), "Direct ink writing of 3D functional materials", *Adv. Funct. Mater.*, **16**(17), 2193-2204.
- Li, H.C.H., Callus, P.J. and Herszberg, I. (2006), "Through-thickness reinforcement repair of delaminated carbon-epoxy panels", *Compos. Struct.*, **75**(1-4), 539-544.
- Maalawi, K. (2011), *Special Issues on Design Optimization of Wind Turbine Structures*: Intech.
- Marín, J.C., Barroso, A., París, F. and Cañas, J. (2009), "Study of fatigue damage in wind turbine blades", *Eng. Fail. Anal.*, **16**(2), 656-668.
- Mishnaevsky Jr, L., Freere, P., Sinha, R., Acharya, P., Shrestha, R. and Manandhar, P. (2011), "Small wind turbines with timber blades for developing countries: Materials choice, development, installation and experiences", *Renew. Energ.*, **36**(8), 2128-2138.
- Motuku, M., Vaidya, U.K. and Janowski, G.M. (1999), "Parametric studies on self-repairing approaches for resin infused composites subjected to low velocity impact", *Smart Mater. Struct.*, **8**(5), 623.
- Norris, C.J., Meadway, G.J., O'Sullivan, M.J., Bond, I.P. and Trask, R.S. (2011), "Self-Healing Fibre Reinforced Composites via a Bioinspired Vasculature", *Adv. Funct. Mater.*, **21**(19), 3624-3633.
- Overgaard, L.C.T., Lund, E. and Thomsen, O.T. (2010), "Structural collapse of a wind turbine blade. Part A: Static test and equivalent single layered models", *Compos. Part A: Appl. S.*, **41**(2), 257-270.
- Pang, J.W.C. and Bond, I.P. (2005), "'Bleeding composites'—damage detection and self-repair using a biomimetic approach", *Compos. Part A: Appl. S.*, **36**(2), 183-188.
- Petrie, E.M. (2007), *Handbook of Adhesives and Sealants, Second Edition*, New York, London: The McGraw-Hill Companies, Inc.
- Shokrieh, M.M. and Rafiee, R. (2006), "Simulation of fatigue failure in a full composite wind turbine blade", *Compos. Struct.*, **74**(3), 332-342.

- Sundaresan, M.J., Schulz, M.J. and A.G. (1999), *Structural Health Monitoring Static Test of a Wind Turbine Blade*. Intelligent Structures and Mechanisms (ISM) Laboratory, Department of Mechanical Engineering, North Carolina A&T State University, Greensboro, North Carolina.
- Tay, T.E., Liu, G., Tan, V.B.C., Sun, X.S. and Pham, D.C. (2008), "Progressive failure analysis of composites", *J. Compos. Mater.*, **42**(18), 1921-1966.
- Timoshenko, S.P. (1941), *Strength of materials Part II*: D. Van Nostrand Company, Inc.
- Trask, R.S. and Bond, I.P. (2006), "Biomimetic self-healing of advanced composite structures using hollow glass fibres", *Smart Mater. Struct.*, **15**(3), 704.
- Williams, H.R., Trask, R.S. and Bond, I.P. (2008), "Self-healing sandwich panels: Restoration of compressive strength after impact", *Compos. Sci. Technol.*, **68**(15-16), 3171-3177.
- Young, S. (2010), Caithness Windfarm Information Forum, [www.caithnesswindfarms.co.uk](http://www.caithnesswindfarms.co.uk). Accessed on 11/12/2014.

BS